JBC RESEARCH ARTICLE

An miRNA derived from amelogenin exon4 regulates expression of transcription factor *Runx2* by directly targeting upstream activators *Nfia* and *Prkch*

Received for publication, July 26, 2021, and in revised form, March 2, 2022 Published, Papers in Press, March 7, 2022,
https://doi.org/10.1016/j.jbc.2022.101807

Rozana Shemirani[1], **Gan Lin**[1], **Dawud Abduweli Uyghurturk**[1], **Michael Le**[2], **and Yukiko Nakano**[1,3,*]

From the [1]*Department of Orofacial Sciences,* [2]*Department of Preventive and Restorative Dental Sciences, and* [3]*Center for Children's Oral Health Research, School of Dentistry, University of California, San Francisco, USA*

Edited by Ronald Wek

Amel*, the gene encoding the amelogenin protein involved in enamel formation, is highly alternatively spliced. When exon4 is excised, it can form a mature miRNA (miR-exon4) that has previously been suggested to indirectly regulate expression of the Runt-related transcription factor 2 (*Runx2*) involved in bone development in ameloblasts and osteoblasts. However, the precise mechanism of this regulation is unclear. In this study, we aimed to identify direct targets of miR-exon4. The transcription factor family nuclear factor I/A (NFI/A) is known to negatively regulate expression of *Runx2* and is among the most highly predicted direct targets of miR-exon4 that link to *Runx2*. Immunostaining detected NFI/A in osteoblasts and ameloblasts *in vivo*, and reporter assays confirmed direct interaction of the Nfia 3′-UTR and miR-exon4. In addition, silencing of *Nfia* in MC3T3-E1-M14 osteoblasts resulted in subsequent downregulation of *Runx2*. In a monoclonal subclone (mi2) of MC3T3-E1 cells wherein mature miR-exon4 was functionally inhibited, we observed significantly downregulated *Runx2* expression. We showed that NFI/A was significantly upregulated in mi2 cells at both mRNA and protein levels. Furthermore, quantitative proteomics and pathway analysis of gene expression in mi2 cells suggested that miR-exon4 could directly target *Prkch* (protein kinase C-eta), possibly leading to RUNX2 regulation through mechanistic target of rapamycin kinase activation. Reporter assays also confirmed the direct interaction of miR-exon4 and the 3′-UTR of *Prkch*, and Western blot analysis confirmed significantly upregulated mechanistic target of rapamycin kinase phosphorylation in mi2 cells. Taken together, we conclude that *Nfia* and *Prkch* expression negatively correlates with miR-exon4-mediated *Runx2* regulation *in vivo* and *in vitro*, suggesting miR-exon4 directly targets *Nfia* and *Prkch* to regulate *Runx2*.

Amelogenin is expressed over the whole body, including osteoblasts (1–3), and exceptionally highly expressed in enamel organs (1). Amelogenin pre-mRNA is highly alternatively spliced producing two major mRNAs for an enamel matrix protein (M180 in mice and H174 in humans) and a signaling protein (leucine-rich amelogenin peptide) (4–7). During this event, exon4 is mostly spliced out (8, 9), and the importance of the spliced out exon4 has not been well investigated. Exon4 sequence is highly conserved among species (10), and we previously reported that a novel miRNA is derived from the spliced out exon4 (miR-exon4) (11).

Mature miRNAs are a class of naturally occurring and small noncoding single-stranded RNA consisting of 18 to 24 nucleotides. They bind to target mRNAs to modulate protein synthesis and mRNA degradation in many organs/tissues, including teeth (12), resulting in altered development, apoptosis, and cell cycle regulation (13). Mammalian miRNA loci reside in introns or exons of their pre-mRNA host genes, sharing promoters, or exist as separate genes transcribed from their own promoters (14). An exonic miRNA is created by the host gene's alternative splicing or through transcription by an independent promoter (15).

In our previous study (11), we confirmed the production of miR-exon4 from the amelogenin gene by transfecting an amelogenin minigene (16), which contains the translated region of mouse *Amel* (exons 2–7 and introns 2–6). *In vivo*, mature miR-exon4 is present in ameloblasts and osteoblasts (11). Nevertheless, we do not know how miR-exon4 contributes to enamel and bone formation yet. As each miRNA can repress hundreds of genes, and one-third of the human genome is estimated to be regulated by miRNAs (17), identifying the direct targets of miR-exon4 is crucial to understanding its role.

Previously, we found that Runt-related transcription factor 2 (*Runx2*) is a downstream target of miR-exon4 in ameloblasts and osteoblasts using cell culture and mouse models (11). Our data showed that reduced miR-exon4 expression resulted in downregulation of *Runx2 in vivo*, and miR-exon4 mimic induced *Runx2* expression *in vitro*. However, in principle, miRNAs function to downregulate target mRNAs through inhibiting translation or inducing degradation. These results are contrary to the principle of the functional mechanism of miRNAs. Thus, we postulated that *Runx2* is not a direct target of miR-exon4. Most likely, miR-exon4 directly regulates another gene, which further negatively regulates *Runx2*.

RUNX2 is a critical and well-established transcription factor for osteoblast differentiation and thus bone matrix formation and mineralization (18) and also enamel mineralization in

* For correspondence: Yukiko Nakano, Yukiko.Nakano@ucsf.edu.

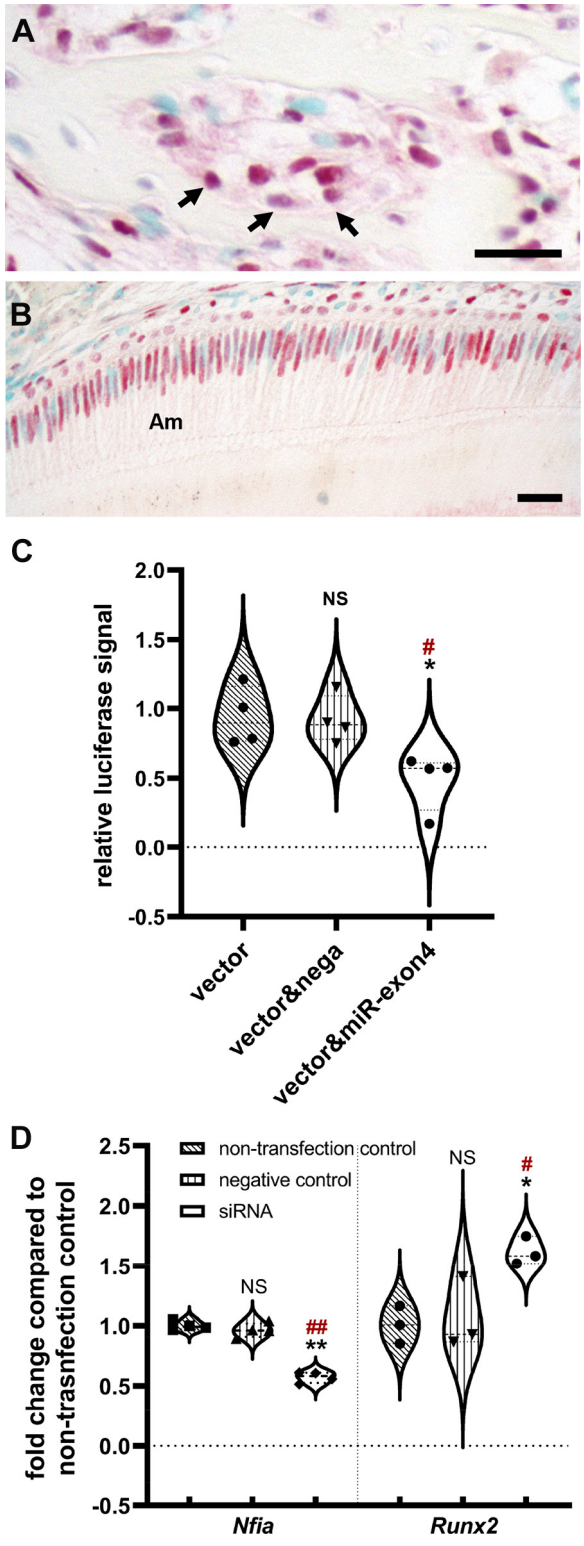

Figure 1. miR-exon4 targets *Nfia*. *A* and *B*, immunohistochemical staining on mixed (C57BL/6J × SJL) mouse bone (*A*) and enamel organ (*B*) shows apparent positive signals on the nucleus of osteoblasts (*A*, *arrows*) and ameloblasts (*B*, Am). Bars represent 25 μm. *C*, incubation of 3′UTR *Nfia* luciferase reporter and miR-exon4 mimic significantly reduced the luciferase activity compared with a reporter only (*$p < 0.05$) and reporter plus negative siRNA (#$p < 0.05$) controls. *D*, when transfection of siRNA for *Nfia* in MC3T3-E1 osteoblasts significantly reduced *Nfia* compared with non-transfection control (**$p < 0.01$) and negative control (##$p < 0.01$). *Runx2* expression is significantly upregulated compared with nontransfection control (*$p < 0.05$) and negative control (#$p < 0.05$). The biological replication of each experimental group is shown as the points in each plot. Statistical significance was analyzed by the two-tailed multiple *t* tests with Bonferroni correction following ANOVA.

humans (19–21) and mice (22). Therefore, in this study, we focused on the axis regulating *Runx2* and attempted to determine the direct target of miR-exon4 using osteoblasts as a model for this axis. We found that miR-exon4 directly targets *Nfia* and *Prkch* (protein kinase C-eta [PKCη gene]) in osteoblasts and further confirmed that it applies in the ameloblasts.

Results

Nfia *is a direct target of miR-exon4*

To identify genes that potentially intermediate between miR-exon4 and *Runx2*, we used a web-based computational prediction algorithm DIANAmicroT 3.0 (http://diana.imis.athena-innovation.gr/DianaTools/index.php?r=site/page&view=software (23)) and screened out 133 potential mouse miR-exon4 targets. Among the potential targets (Data S1), we further selected the molecules that may negatively regulate *Runx2* expression by Ingenuity pathway analysis (IPA) (Qiagen). *Nfia* was a molecule with the highest score among those associated with *Runx2* and was the only one known to negatively regulate *Runx2* mRNA (in total fifth top score of 133 miR-exon4 candidates) (24). Immunostaining showed nuclear factor I/A (NFI/A) protein in osteoblasts (Fig. 1*A*) and ameloblasts (Fig. 1*B*), suggesting a possible direct regulation of *Nfia* by miR-exon4 in those cells. We examined the interaction of miR-exon4 and *Nfia* using *in vitro* miRNA target validation reporter assay to test this possibility. We found a significant reduction of the luciferase reporter signal derived from the plasmid vector, which contained 3′UTR of *Nfia,* when adding miR-exon4 mimic compared with without miR-exon4 mimic and negative control oligonucleotide (Fig. 1*C*). It indicates that miR-exon4 regulates *Nfia* by directly binding to the 3′UTR. NFI/A is known to bind the cell-specific protected region in the *Runx2* promoter and represses the promoter activity of *Runx2* in osteoblasts (24). To further confirm NFI/A-*Runx2* regulation, we silenced *Nfia* in MC3T3-E1 osteoblasts and observed significantly upregulated *Runx2* expression (Fig. 1*D*).

Osteoblast as a model to test a pathway from miR-exon4 to Runx2

In search of the *in vitro* model investigating the miR-exon4-*Runx2* axis, we found in our preliminary study that existing ameloblast-like cell culture models did not react to the loss of miR-exon4 as they expressed a low level of amelogenin as well as miR-exon4 (data not shown). Also, those cell culture models cannot go through the cell differentiation process forming enamel matrix, like *in vivo*. Thus, we aimed to use osteoblast culture as a model to analyze the miR-exon4 to RUNX2 pathway as we previously confirmed the presence of miR-exon4 in mouse osteoblasts (11), and RUNX2 is a well-known regulator of osteoblast differentiation. To validate the use of osteoblast culture for miR-exon4 study, we first examined the expression profile of miR-exon4 in a mouse

calvarial primary osteoblast culture. miR-exon4 was present in the *Amel* WT primary osteoblasts throughout the culture period, and the level of miR-exon4 was higher at the earlier culture period (Fig. 2*A*, *black*). The *Runx2* expression pattern goes up in the same culture period as differentiation progresses (Fig. 2*B*, *black*).

Previously Atsawasuwan *et al.* (1) reported that primary osteoblasts of *Amel* KO mice show significantly reduced *Runx2* mRNA, whereas those in calvariae *in vivo* were the same as WT. Similar to their findings, our primary osteoblast culture of *Amel* KO mice expressed significantly reduced mRNA of *Runx2* at days 3 and 9 of the culture (Fig. 2*B*, *orange*), whereas *in vivo*, *Runx2* expression was maintained as the WT in osteoblasts directly harvested from calvariae (11). Moreover, in this study, we observed that miR-exon4 in *Amel* KO primary osteoblasts was significantly downregulated at all three points of the culture period compared with the WT primary osteoblasts (Fig. 2*A*, *orange*). Considering miR-exon4 expression level in *Amel* KO osteoblasts *in vivo* somehow maintained at the same level of WT (11), change in miR-exon4

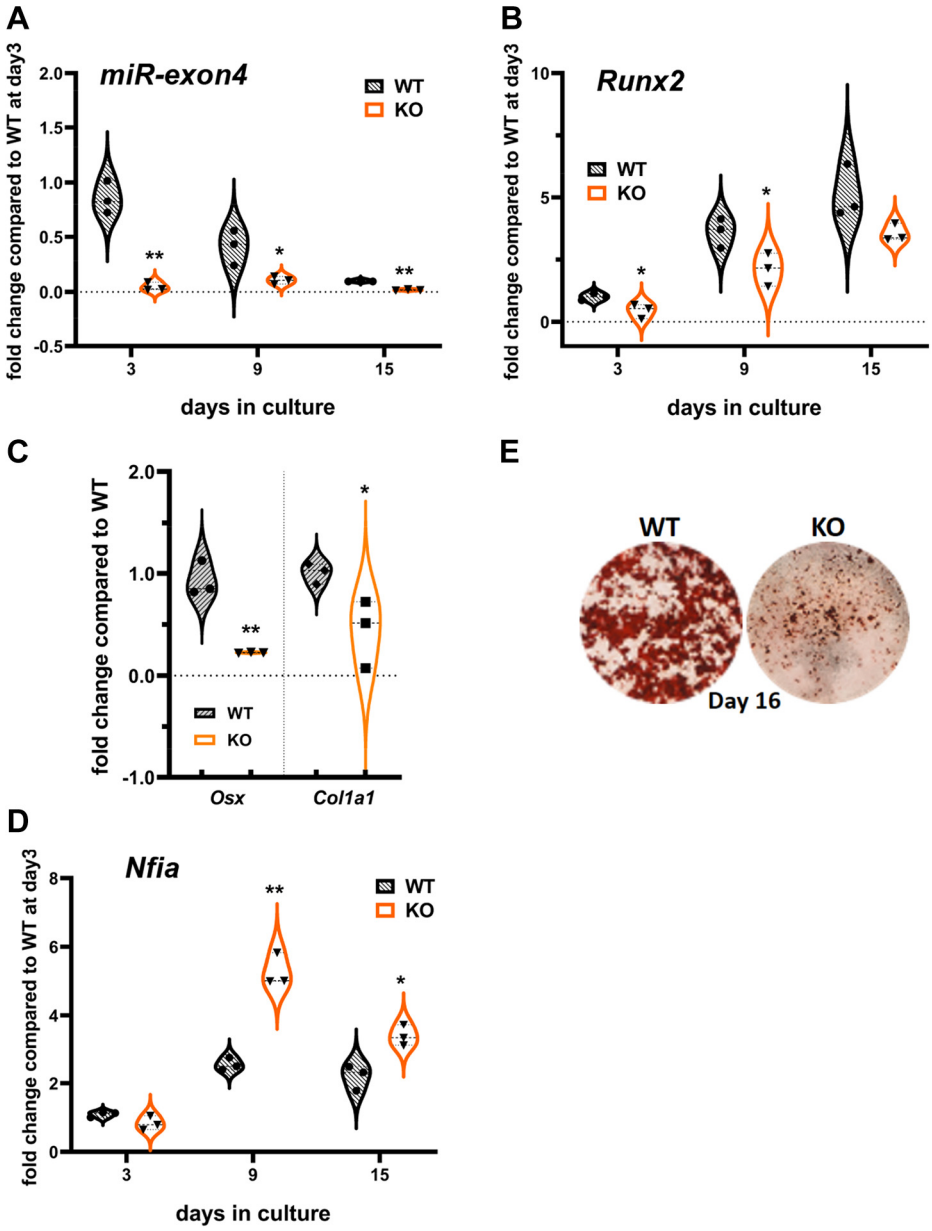

Figure 2. miR-exon4 in primary osteoblast culture. *A*, expression of mature miR-exon4 is at the highest level on day 3 and goes down as differentiation progresses in *Amel* WT (in *black*). miR-exon4 expression in *Amel* KO primary osteoblasts is significantly reduced compared with WT in each culture point (*orange*). *$p < 0.05$, **$p < 0.01$. *B*, *Runx2* expression in *Amel* WT primary osteoblasts goes up as the culture period goes by (in *black*). On days 3 and 9 of the culture, *Runx2* expression in *Amel* KO primary osteoblasts is significantly downregulated compared with WT (in *orange*). *$p < 0.05$. In the day 3 primary osteoblasts of *Amel* KO mice, *Osx* and *Col1a1* expression are significantly downregulated compared with the WT (*$p < 0.05$, **$p < 0.01$). *C*, on day 16 of culture, the primary osteoblast culture of *Amel* KO mice shows apparently reduced Alizarin Red–positive mineral nodules compared with the WT. *D*, *Nfia* expression in *Amel* KO was significantly upregulated at days 9 (**$p < 0.01$) and 15 (*$p < 0.05$) of culture compared with the WT. The biological replication of each experimental group is shown as the points in each plot. Statistical significance was analyzed by independent Student's *t* tests following *F* test.

expression pattern looked like synchronizing to *Runx2* expression in osteoblasts. The likely correlating reduction of miR-exon4 and *Runx2* also happens in mouse enamel organs of *Amel* KO mouse *in vivo* (11), suggesting osteoblast culture is an appropriate *in vitro* model to examine the miR-exon4-*Runx2* axis. This system also showed downregulation of osterix (*Osx*) and collagen type I alpha 1 chain, osteoblast differentiation markers and direct downstream molecules of *Runx2* (Fig. 2*C*), and reduced bone nodule formation (Fig. 2*D*). Expression of *Nfia* was significantly upregulated at days 9 and 15 of culture but not at day 3 (Fig. 2*E*). Since *Amel* KO culture also lacks amelogenin protein, which has signaling functions and induces osteogenesis (4), the absence of amelogenin protein possibly influences the change in molecular activity. Therefore, we aimed to explore the miR-exon4-*Runx2* axis in osteoblasts that only miR-exon4 is inhibited in the following studies.

Inhibition of miR-exon4 resulted in downregulation of Runx2 *without changing cell viability*

To explore the pathway from miR-exon4 to *Runx2* in a stable and reproducible osteoblast culture system, we tested the effect of lacking active miR-exon4 using MC3T3-E1 subclone M14 osteoblasts. The subclone M14 is known to differentiate with clearly distinct stages, and the extracellular matrix mineralizes as bone nodules by supplementing ascorbic acid (AA) and beta-glycerophosphate (βGP) in the culture medium (25). In the passage range we used in this study (passage 20–30), cells went through differentiation and matrix deposition stage during days in the culture of 0 to 15 and formed mineralized bone nodule after day 15. Throughout the 27 days of the culture period, the alkaline phosphatase (ALPase) activity of the culture increased (Fig. S1). Like the primary osteoblasts, MC3T3-E1 M14 osteoblasts expressed miR-exon4 in the entire culture period, with the highest level at the culture day 3 and lowest at day 15. Expression of *Runx2* showed a similar profile of miR-exon4 (Fig. 3*A*).

Using MC3T3-E1 M14 osteoblasts, we further generated monoclonal subclones, in which mature miR-exon4 was permanently inhabited by the miR-exon4 inhibitor delivered *via* a lentiviral vector. Subclones mi2 and mi4 were selected among the 10 subclones according to the inhibition level of *Runx2* expression at day 3 of the culture (Fig. 3*B*). Later, on days 9, 15, and 21 of culture, *Runx2* expression was consistently suppressed in the subclone mi2 compared with nontransduced control and negative control, whereas the subclone mi4 did not show the significant suppression of *Runx2* at days 15 and 21 (Fig. 3, *C*–*E*). The subclone mi2 also did not show any change in cell viability throughout the culture compared with the controls. In contrast, the viability of mi4 was moderately but significantly reduced at days 9 and 23 (Fig. 3*F*). On day 3 of culture, expression of *Osx* was also significantly suppressed in both mi2 and mi4 (Fig. 3*G*). We selected the subclone mi2 for the subsequent studies as it showed the most stable *Runx2* reduction associated with the lack of active miR-exon4.

Inhibition of miR-exon4 resulted in upregulated NFI/A protein in the subclone mi2

To examine if the lack of active miR-exon4 affects NFI/A, NFI/A was detected in the total protein extract at days 3 and 9 of culture (Fig. 4, *A* and *C*). Western blotting and following intensity analysis normalized with the total protein showed significantly upregulated NFI/A protein in the subclone mi2 compared with the nontransduced control at day 9 of culture (Fig. 4*D*) but not at day 3 (Fig. 4*B*). As an miRNA suppresses the translation of target mRNA to protein and also causes decay of the target mRNA (26–29), we also examined the level of *Nfia* mRNA. Consistent with protein, *Nfia* mRNA level was not significantly changed in the subclone mi2 at day 3 (Fig. 4*E*), whereas at day 9, *Nfia* was significantly upregulated compared with controls (Fig. 4*F*). On day 15, *Nfia* mRNA level was also significantly upregulated in mi2 compared with the controls (Fig. S2). These data indicate that miR-exon4 targets *Nfia* at day 9 and likely day 15 of osteoblast differentiation. The not significant change in NFI/A protein and mRNA levels observed in day 3 culture of mi2 osteoblasts suggests stage-specific interaction of miR-exon4 and its targets during osteoblast differentiation.

miR-exon4 also targeted Prkch *to regulate* Runx2 *expression in osteoblasts*

To further explore the miR-exon4 targets at the earlier stage of the osteoblast culture, quantitative proteomics analysis was performed using the total protein extracts of cells at day 3 in the culture. It identified 58,704 peptides and 5283 proteins (Data S2), among which 53 proteins were significantly upregulated (fold change >1.5; $p < 0.05$). Comparing genes for these proteins with the computationally predicted direct targets of miR-exon4 in human and mouse genes (DIANAmicroT 3.0), 32 genes in mice and 20 genes in humans (37 genes in total) were commonly included (Fig. 5*A*). Associations of these common genes with *Runx2* were then analyzed by IPA (Qiagen). We first confirmed that none of the 37 genes and their translated proteins directly associate with *Runx2*. Therefore, we attempted to find the indirect association of candidate miR-exon4 and *Runx2* using proteomics data of mi2. IPA causal network analysis found that among the affected canonical pathways in the mi2, 349 molecules were found in the overlapping pathways that share the common genes participating with at least one other pathway. Among 349 molecules, five molecules (Ppp2r1b, Myl9, Prkch, Dnajc21, and Myl12a) were with fold change >1.5 in differential expression analysis of proteomics, and four of them (*Ppp2r1b*, *Myl9*, *Prkch*, and *Dnajc21*) were common in mouse and human. Thus, these four molecules were the most plausible miR-exon4 direct targets. The possible pathways from the four molecules to RUNX2 were built by the IPA and applied to IPA expression analysis of mi2. Comparing the $-\log(p \text{ value})$: 5.306 (*Prkch*), 2.083 (*Ppp2r1b*), 2.024 (Myl9), 1.272 (*Dnajc21*) ($p < 0.05$, $-\log(p \text{ value}) > 1.30$ is significant by Fisher's t test), we selected PKCη mRNA (*Prkch*) as the molecule with the highest $-\log(p \text{ value})$ to further explore the possible pathway link to

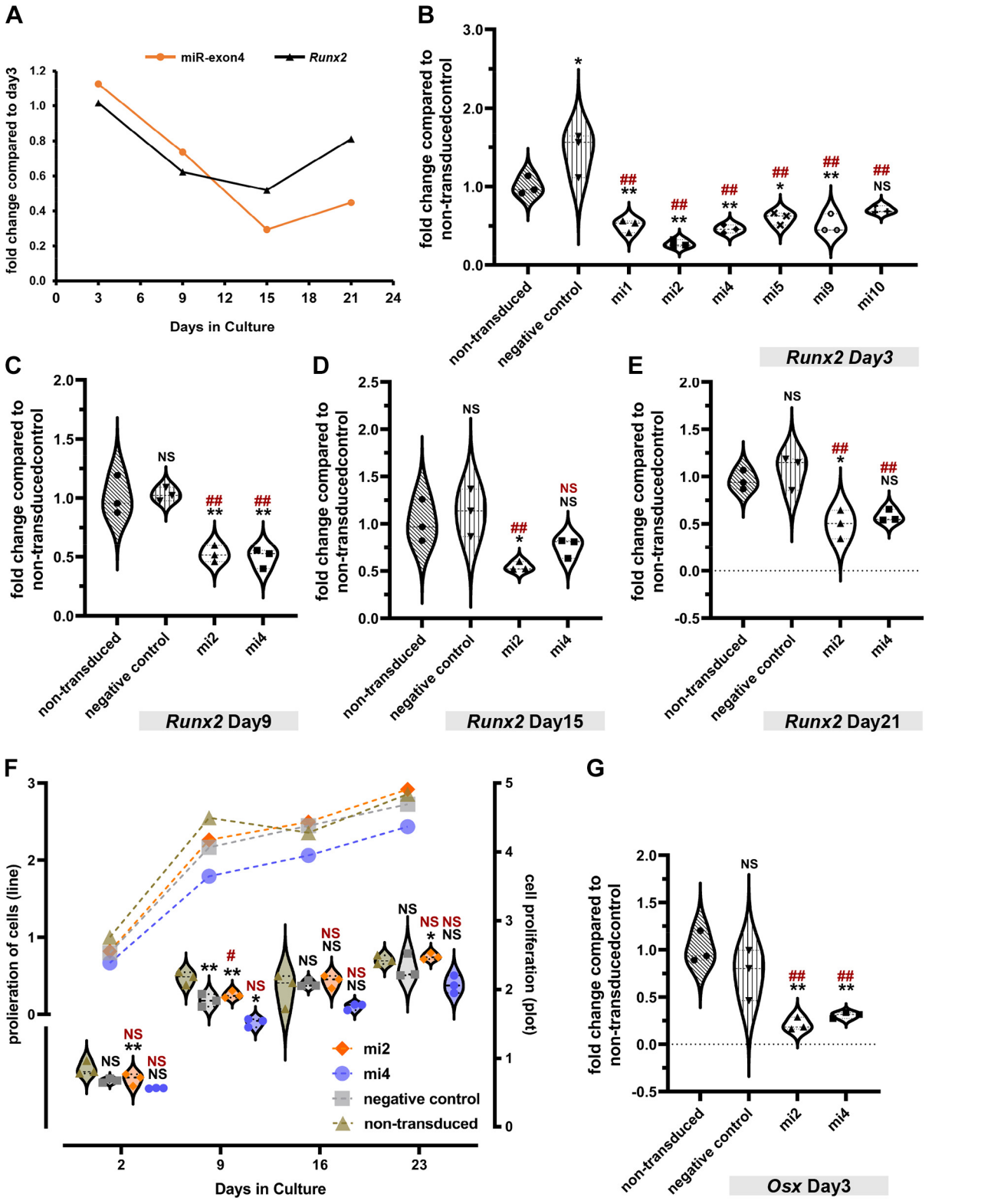

Figure 3. Monoclonal subclones of MC3T3-E1 M14 osteoblasts that miR-exon4 is functionally inhibited. *A*, expression of miR-exon4 and *Runx2* in MC3T3-E1 M14 osteoblasts. Both of them are expressed at the highest level on day 3 of culture and go down as the cells differentiate. *B*, *Runx2* mRNA level in the monoclonal subclones of MC3T3-E1 M14 osteoblasts at day 3 in culture. All subclones except mi10 show significant (*$p < 0.05$, **$p < 0.01$) reduction in *Runx2* compared with the nontransduced control. All subclones show a significantly reduced (##$p < 0.01$) *Runx2* mRNA level than the negative control. *C–E*, later, at days in culture 9, 15, and 21, subclone mi2 shows consistent reduction of *Runx2* mRNA compared with nontransduced control (*$p < 0.05$, **$p < 0.01$) and negative control (##$p < 0.01$). *F*, cell proliferation of subclone mi2 does not significantly differ from the nontransduced control (*$p < 0.05$ except day 9) and negative control throughout the culture period. *G*, *Osx* mRNA level is also significantly reduced in subclones mi2 and mi4 compared with nontransduced control (**$p < 0.01$) and negative control (##$p < 0.01$). Statistical significance was analyzed by the two-tailed multiple *t* tests with Bonferroni correction following ANOVA. The biological replication of each experimental group is shown as the points in each plot.

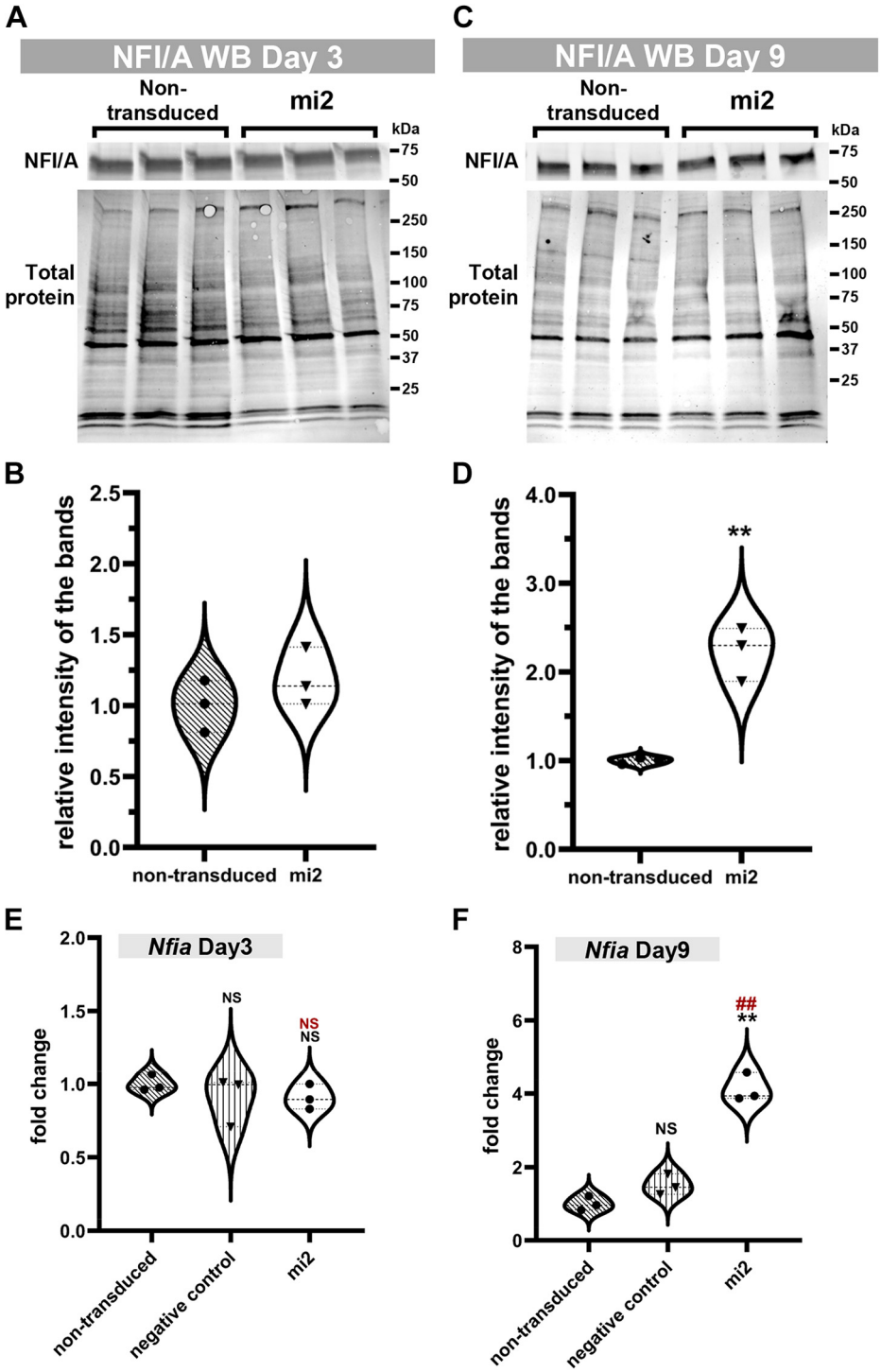

Figure 4. Protein and mRNA levels of NFI/A in subclone mi2. Western blotting for NFI/A at day 3 (*A* and *B*) and 9 (*C* and *D*). The intensity of each band for NFI/A was normalized by the corresponding lane's total protein (*A* and *C*). The normalized intensity compared between nontransduced and mi2 (*B* and *D*) demonstrates significant upregulation of NFI/A in mi2 at day 9 (*$p < 0.05$) but not at day 3. Statistical significance was analyzed by independent Student's *t* tests following *F* test. Consistent with protein, *Nfia* mRNA was also upregulated in the subclone mi2 at day 9 compared with nontransduced control (**$p < 0.01$) and negative control (##$p < 0.01$) (*F*), whereas there is no change in the samples of day 3 (*E*). Statistical significance was analyzed by the two-tailed multiple *t* tests with Bonferroni correction following ANOVA. The biological replication of each experimental group is shown as the points in each plot.

Runx2. Overlaying the predicted upregulation/downregulation and actual fold change of the proteomics analysis to the possible pathway from PKCη to RUNX2 in IPA, we found a most plausible cascade shown in Figure 5*B* (*top*). If this predicted chain of reactions happens, *Prkch* has to be a direct target of miR-exon4, and mechanistic target of rapamycin kinase (mTOR) must be phosphorylated at Ser2448. As 3′UTR of *Prkch* was the predicted binding site of miR-exon4 in the

A

Overlapped with mouse miR-exon4 targets	Overlapped with human miR-exon4 targets	Fold Change	p-value
Tnn	Tnn	2.657	0.00000304
Gas2	Gas2	2.039	0.00000541
Mad2l1	Mad2l1	2.017	0.00000466
Prrx1	Prrx1	1.913	0.00000980
Ncam1	Ncam1	1.800	0.00003868
Tmx2	Tmx2	1.738	0.00001106
Ncam1	Ncam1	1.716	0.00002128
Cyp26b1	Cyp26b1	1.685	0.00006463
Prkch	Prkch	1.645	0.00107507
Sgcb	Sgcb	1.626	0.00000971
Dnajc21	Dnajc21	1.612	0.00073533
Krt13	Krt13	1.601	0.13452212
Tmem65	Tmem65	1.557	0.00013652
Cavin1	Cavin1	1.518	0.00001796
Fstl1	Fstl1	1.511	0.00013649
	Lum	1.972	0.00000526
	Tpm1	1.830	0.00000472
	Sdc2	1.750	0.00000122
	Krt79	1.727	0.10099947
	Ggt7	1.544	0.00005532
Ahnak2		2.761	0.00000375
Abi3bp		2.668	0.00000157
Myof		2.414	0.00005499
Col6a3		2.378	0.00034428
Sgce		1.898	0.00000165
Rgs17		1.880	0.00000873
Dkk3		1.792	0.00000028
Ahr		1.790	0.00007613
Cald1		1.755	0.00002594
Hmga2		1.720	0.00017184
Cavin4		1.688	0.00003974
Ptn		1.599	0.00000606
Myl12b		1.554	0.00056427
Tagln		1.548	0.00000494
Thbs2		1.524	0.00000462
Ctsb		1.511	0.00006929
Thbs2		1.510	0.00009563

Genes for FC>1.5 proteins overlapped with DIANA microT miR-exon4 target mouse or human

B

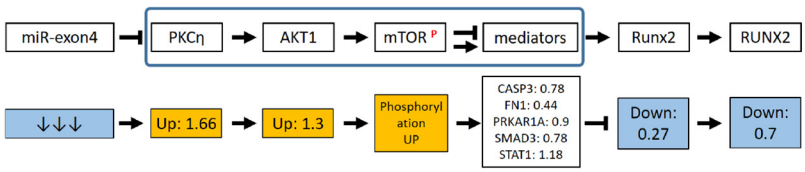

C

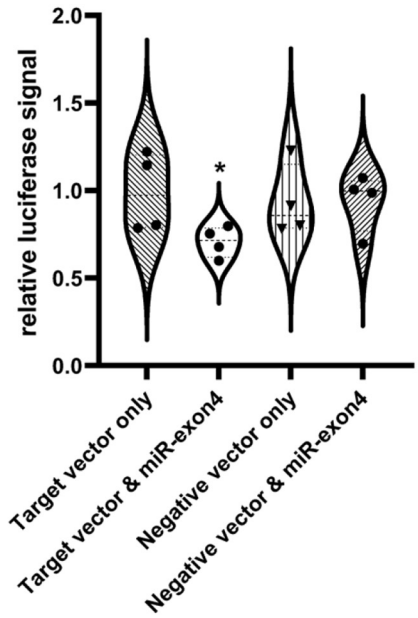

D

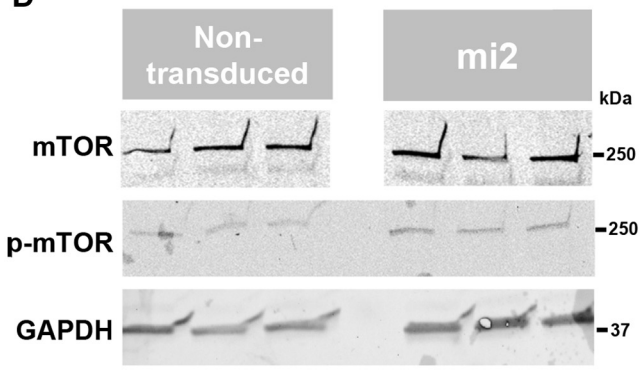

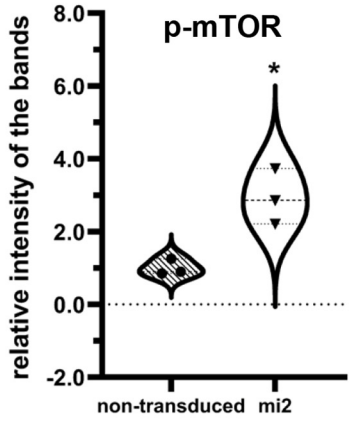

Figure 5. miR-exon4 induces mTOR activation *via* PKCη. *A*, list of gene names commonly found in proteomics data (fold change >1.5) and predicted human or mouse miR-exon4 targets. Fold change and *p* value are from proteomics. *B*, a potential signaling cascade from miR-exon4 to RUNX2 (*top*). *Bottom*, Actual upregulation (in *yellow*) and downregulation (in *blue*) in subclone mi2 at day 3 of culture. Each number indicates fold change detected in proteomics or qPCR analysis. *C*, Luciferase reporter activity derived from a vector with *Prkch* 3′UTR. The presence of miR-exon4 significantly suppresses the luciferase activity in the cell culture with a reporter vector with *Prkch* 3′UTR. ($p < 0.05$). miR-exon4 mimic does not change the luciferase reporter signal in the cell culture with the negative control vector. *D*, Western blotting of mTOR and phosphorylated mTOR in the day 3 osteoblast extracts. Quantification analysis after the normalization with GAPDH bands showed that phosphorylated mTOR is significantly upregulated in mi2 ($p < 0.05$). Image of mTOR Western blotting is split at the border of nontransduced control and mi2 for the presentation purpose. The biological replication of each experimental group is shown as the points in each plot. Statistical significance was analyzed by independent Student's *t* tests following *F* test. mTOR, mechanistic target of rapamycin kinase.

computational analysis, we examined the binding between miR-exon4 and 3′UTR *Prkch* by a luciferase reporter assay. It confirmed the significant reduction of the luciferase reporter signal when mixing with the miR-exon4 mimic (Fig. 5*C*). Western blotting analysis using the protein extract of the mi2 at day 3 showed significant upregulation of Ser2448 phosphorylated mTOR (Fig. 5*D*), while no change in mTOR. Together, these data suggest that when miR-exon4 is inhibited, PKCη-driven mTOR activation occurs. It further changes the expression of mediators, which results in downregulation of *Runx2* expression (Fig. 5*B*, *bottom*).

Nfia *and* Prkch *mediated miR-exon4*-Runx2 *axis in both osteoblasts and ameloblasts* in vitro *and* in vivo

To examine if *Nfia* and *Prkch* also mediate the miR-exon4-*Runx2* axis in ameloblasts, we measured *Nfia* and *Prkch* mRNA expression in our previously published ameloblast model systems in which miR-exon4 expression was altered (11). In support of the changes seen in osteoblasts *in vitro*, the miR-exon4-related upregulation in *Nfia* and *Prkch* mRNA was observed *in vivo* in the enamel organ of postnatal 5 (P5) *Amel* KO mice, a model lacking miR-exon4 in enamel organ (11), compared with WT (Fig. S3). Also, *in vitro,* when miR-exon4 mimic was transiently transfected and caused *Runx2* upregulation (11), LS8 ameloblastic cells showed downregulation of *Nfia* and *Prkch* (Fig. S4). Furthermore, in osteoblasts of *Amel* KO mice *in vivo*, where miR-exon4 expression did not change, *Runx2* (11), *Nfia*, and *Prkch* were also unchanged compared with the WT (Fig. S5). Whereas in the primary osteoblast culture, where miR-exon4 and *Runx2* were downregulated in the *Amel* KO (Fig. 2, *A* and *B*), *Nfia* was upregulated at days 9 and 15 of culture (Fig. 2*D*), and *Prkch* was upregulated at day 3 (Fig. S6). The changes in expression of miR-exon4, *Runx2*, *Nfia*, and *Prkch* in the two cell types *in vivo* and *in vitro* were summarized in Figure 6. The consistency of correlated expression patterns of miR-exon4, *Runx2*, *Nfia*, and *Prkch* throughout our model systems indicates that *Nfia* and *Prkch* mediate the miR-exon4-*Runx2* axis in both osteoblasts and ameloblasts.

Discussion

We previously reported that alternative splicing of amelogenin pre-mRNA produces a new type of derivative, miR-exon4, from spliced out exon4 (11). Considering the importance of the amelogenin gene in dental enamel formation and the high rate (80%) of exon4 spliced out during the amelogenesis (11), a certain contribution of miR-exon4 was expected. Identifying the direct targets and pathways that miR-exon4 is involved in is crucial in order to understand the biological role of miR-exon4. As our previous *in vivo* and *in vitro* study suggests the possible indirect regulation of *Runx2* by miR-exon4 in osteoblasts and ameloblasts (11), we chose the molecular cascade from miR-exon4 to *Runx2* to examine in this follow-up study.

Our first candidate target of miR-exon4 was *Nfia*. NFI/A belongs to the NFI protein family, which function as cellular transcription factors for multiple genes by forming homodimers or heterodimers. NFI/A is known to bind the cell-specific protected region in the *Runx2* promoter and represses the promoter activity of *Runx2* (24). Although Zambotti *et al.* reported that the UMR106 osteoblast culture did not express *Nfia* mRNA, here in our study, NFI/A protein was detected in osteoblasts and ameloblasts *in vivo* by immunostaining. Also, the presence of NFI/A protein and mRNA was confirmed in MC3T3-E1 osteoblast culture. In ameloblasts, gene expression of *Nfia* is also confirmed throughout the ameloblast differentiation according to the microarray data of mouse and rat enamel organ available at the National Center for Biotechnology Information microarray database (Gene Expression Omnibus accession numbers: GSE59401

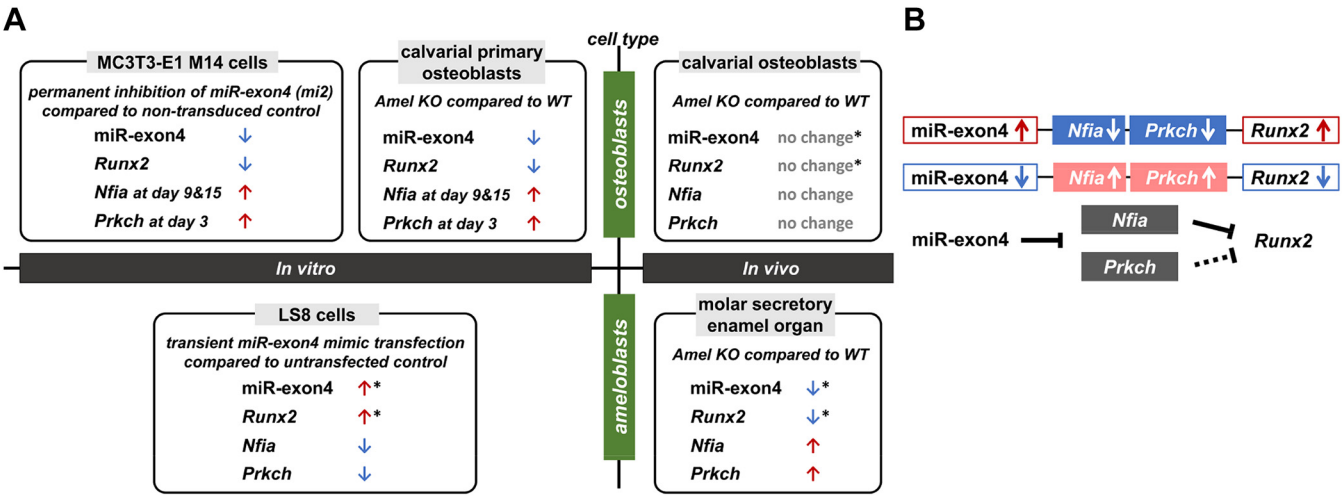

Figure 6. Summary of miR-exon4, *Runx2*, *Nfia*, and *Prkch* expression and molecular cascade. *A*, changes in miR-exon4 and mRNA expression, which were observed under the different genetic and experimental conditions in osteoblasts and ameloblasts *in vivo* and *in vitro*, are summarized. In all experimental models, when miR-exon4 expression changes, *Runx2*, *Nfia*, and *Prkch* also change accordingly. *Previously published data (11). *B*, the four molecule's expression changes are summarized in the miR-exon4-*Runx2* axis (*top*). It supports the suggested regulatory relationship of the molecules in the axis confirmed through the experiments (*bottom*). *Solid line*: direct regulation; *dashed line*: indirect regulation.

(30) and GSE57224 (31)). In addition, considering the significant role of another NFI family member protein, NFI/C, in bone and teeth formation (32–34), it is possible the NFI/A also plays a pivotal role in bone and enamel formation. Nevertheless, the exact role of NFI/A both in osteoblast and ameloblasts is not well known yet.

In this study, our reporter assay confirmed the direct interaction of miR-exon4 and *Nfia*. The upregulation of NFI/A protein and *Nfia* mRNA in the osteoblast culture lacking the functional miR-exon4 also supports *Nfia* as a direct target of miR-exon4. Thus, we propose a cascade that miR-exon4 regulates NFI/A, which further negatively regulates *Runx2* expression. A possibility that this cascade also happens *in vivo* is supported by the observation of a significantly upregulated *Nfia* expression in P5 *Amel* KO enamel organ, an *in vivo* model of reduced miR-exon4 and *Runx2* in enamel organ, compared with WT.

miRNA is known to cooperate with transcriptional factors and regulate target molecules' expression in the developmental stage-specific manner by forming feedback loops (35, 36). This functional mechanism seems universal from plant to mammals, including craniofacial tissue development of mice (37, 38). In this study, we also observed the significant regulation of *Nfia* by miR-exon4 in a specific culture period of MC3T3-E1 osteoblasts. If miR-exon4 targets *Nfia* throughout the culture and is an absolute regulator, the expression profile of these two molecules would be opposite as the culture period goes by. However, the expression profile of *Nfia* mRNA in MC3T3-E1 osteoblasts shows a similar pattern as miR-exon4 and *Runx2* (data not shown), suggesting miR-exon4 targets *Nfia* not throughout the differentiation but at a limited time.

Prkch is another target of miR-exon4 direct we identified in this study. Compared with the direct relation of NFI/A and *Runx2*, the proposed cascade from *Prkch* to *Runx2* is more complicated and indirect. Thus, the general application of this cascade other than the MC3T3-E1 cell culture is not certain. However, the correlated expression profile of miR-exon4, *Runx2*, and *Prkch* in ameloblasts indicates the possibility that this cascade also commonly works in multiple cells and tissues. Specially, the upper half of the cascade, PKCη-driven mTOR activation, is more direct and could happen in different cells and tissues. mTOR signaling is known to have substantial roles in skeletal development, including stimulating osteoblast differentiation (39, 40). Pathway analysis of our proteomics data shows that mTOR signaling, including 76 molecules, is one of the significantly changed canonical pathways in subclone mi2 compared with the control ($p < 3.95E-15$, activation z score = 0.603). Although PKCη is the only confirmed direct target of miR-exon4 among the 76 molecules, all 37 upregulated molecules among the 76 molecules are listed in the computationally predicted miR-exon4 targets. The fold change of these 37 molecules is less than 1.5. However, considering the mild effect (less than 2–3 fold change) of an miRNA on the individual target genes (27, 41–43), also that the magnitude of the change in target mRNA level depends on the abundance of the target mRNA (26), these 37 molecules are also possibly targeted by miR-exon4. Thereby, the considerable contribution of miR-exon4 in regulating mTOR signaling and further osteoblast differentiation is suggested.

RUNX2 is a critical transcription factor for osteoblast differentiation (18) by regulating multiple downstream genes, including *Osx*. Mutations in the *Runx2* gene are also known to cause heredity enamel defects (19–21). In teeth, RUNX2 is known to negatively regulate Sonic hedgehog (SHH) signaling (44), which has an important role in the ameloblast differentiation at the early stages of development (45, 46). RUNX2 also regulates both odontogenic ameloblast–associated protein (ODAM) expression and amelotin promoter activity (47, 48) in ameloblasts. Our previous report found significantly upregulated *Shh* mRNA expression and downregulation of *Odam* and amelotin mRNAs in secretory-stage enamel organs compared with WT (11). In ameloblasts, RUNX2 also regulates *Amel* expression, resulting in enamel defects (22). Thus, a substantial role of *Runx2* is suggested in ameloblast differentiation, like in osteoblasts.

In this study, we focused on RUNX2 as a downstream of miR-exon4 and investigated the direct targets of miR-exon4 employing the similar importance of RUNX2 in both osteoblasts and ameloblasts. *Amel* KO mouse is a model of reduced miR-exon4 in ameloblasts (11). However, in osteoblasts directly harvested from *Amel* KO mice, while *Amel* mRNAs are still downregulated, miR-exon4 and *Runx2* expression is maintained at the same level of WT (11), supporting the reported mild bone phenotype in *Amel* KO mice (1). Interestingly, however, in primary osteoblast culture, the expression level of miR-exon4 and *Runx2* and bone nodule formation were significantly reduced in *Amel* KO compared with WT. Although the reason for the discrepancy between *in vivo* and *ex vivo* is not apparent and yet to be investigated, these data also support the potential correlation of miR-exon4 and *Runx2*.

The connection between miR-exon4 and *Runx2* found in this study suggests the significant roles of miR-exon4 in osteoblast and ameloblast differentiation. Quantitative proteomics analysis, which detected multiple proteins upregulated by miR-exon4 inhibition, indicates more direct targets of miR-exon4 besides *Nfia* and *Prkch*. With further investigation of these upregulated molecules in the future, the functional mechanisms and significance of miR-exon4 will be more clarified.

Experimental procedures

Animal

Amel WT mice that were maintained as mixed mice (C57BL/6J × SJL) and *Amel* KO mice (a kind gift from Dr Carolyn Gibson, University of Pennsylvania) (49) colonies were maintained at the University of California, San Francisco (UCSF) animal facility. The UCSF Animal Care Committee approved the animal handling protocol. At P5, mice were euthanized, and mandibles were dissected for immersion fixation in 4% paraformaldehyde in a 0.06 M sodium cacodylate buffer (pH 7.3) at 4 °C for 24 h. After decalcification in 8% EDTA (pH 7.3), samples were processed for routine paraffin

embedding and sectioning. For some mice, calvariae were harvested and processed for primary osteoblast culture. Also, calvarial osteoblasts and molars were harvested from some mice for total RNA extraction as described previously (11).

Immunohistochemistry and imaging

Longitudinal sections of the mixed (C57BL/6J × SJL) mouse mandibles were deparaffinized and then incubated with 10% swine and 5% goat sera, followed by incubation with primary antibodies, rabbit anti-NFI/A (Thermo Fisher Scientific; catalog no.: PA5-35936) overnight at room temperature. A biotinylated swine anti-rabbit immunoglobulin G F(ab')2 fraction (Dako Cytomation; catalog no.: E0431) was used as the secondary antibody for 1 h at room temperature incubation, followed by incubation with ALPase-conjugated streptavidin (Vector Laboratories, Inc) for 30 min. According to the manufacturer's instructions, the immunoreaction was visualized with the Vector Red Alkaline Phosphatase Substrate Kit (Vector Laboratories, Inc). Levamisole (1 mM) was added to the reagents as an inhibitor for endogenous tissue nonspecific ALPase. Counterstaining was done with methyl green. Normal rabbit or mouse serum immunoglobulin G was used in negative controls. Immunoreactions were observed under a light microscope (Nikon E800 System; Nikon TMS) and photographed using Q Capture Imaging software to evaluate staining intensity. Adobe Photoshop software (Adobe Systems, Inc) was used to adjust image contrast minimally. Image analysis was independently assessed and compared by two separate investigators.

Luciferase reporter assay

Two dual reporter vectors encoding, SV40 promoter–driven MetLuc (Metridia luciferase) followed by entre 3′UTR of mouse *Nfia* and CMV promoter–driven enhanced GFP (EGFP) (Vector Builder), and SV40 promoter–driven secreted GLuc (Gaussia luciferase) followed by entire mouse *Prkch* 3′UTR and CMV promoter–driven secreted alkaline phosphatase (SEAP) (GeneCopoeia), were used.

Human embryonic kidney 293T/17 cells (UCSF Cell and Genome Engineering Core) were plated at an initial density of 156,250 cells/cm^2 and cultured with Dulbecco's modified Eagle's medium with GlutaMAX supplemented with 10% fetal bovine serum (FBS) and 1% penicillin/streptomycin (P/S) for 24 h at 37 °C with 5% CO_2. For *Nfia* reporter assay, the reporter vector and miScript miR-exon4 mimic (n = 4) (ACUGACAGGACUGCAUUA; Qiagen) or AllStars Negative Control siRNA (n = 4) (Qiagen) were cotransfected using Lipofectamine 2000 (Thermo Fisher Scientific). The reporter vector-only (n = 4) transfection was used as the control. For the *Prkch* reporter assay, a dual reporter vector (n = 4) or universal negative control vector (n = 4) (GeneCopoeia) was cotransfected with the miR-exon4 mimic using Lipofectamine 2000. The dual reporter vector-only (n = 4) or universal negative control vector-only (n = 4) transfection was used as the controls. After 48 h of culture at 37 °C, MetLuc activity in the culture medium was measured using Ready-To-Glow Secreted Luciferase Reporter Assay (Takara Bio). According to the manufacturer's instruction, the secreted GLuc and SEAP in the culture medium was measured using Secrete-Pair Dual Luminescence Assay Kit (GeneCopoeia). EGFP signal in the cells was measured by a fluorescent mode (excitation/emission 488 nm/508 nm) of SpectraMax iD3 multimode microplate reader (Molecular Devices). The measured luciferase activity of each sample was normalized by measuring EGFP (for *Nfia* reporter) or SEAP (for *Prkch* reporter), internal control for transfection. For the *Nfia* reporter assay, the difference in the signal was analyzed among reporter vector only, reporter vector and miR-exon4 mimic, and reporter vector and negative control by the two-tailed multiple t tests with Bonferroni correction following ANOVA (50). For the *Prkch* reporter assay, the difference in the signal between with and without miR-exon4 was analyzed for each test vector and negative control vector by independent Student's t test following F test. For both analyses, $p < 0.05$ was considered significantly different.

Primary osteoblast culture

Dissected calvariae from *Amel* WT and KO were trimmed off to remove cartilaginous elements, and the frontal bones were kept for scrape cleaning of both sides of the bone. The cleaned bone pieces were digested in alpha minimum essential medium (αMEM) without AA (Thermo Fisher Scientific) containing 0.1 mg/ml collagenase P (Sigma–Aldrich) and 1:40 diluted trypsin (Genesee Scientific) at 37 °C with two times digestion medium changing. Digested bone pieces were cultured in a plate containing αMEM supplemented with 10% FBS and 1% P/S at 37 °C with 5% CO_2 for 4 days. The plate was then treated with trypsin to collect the primary osteoblasts for seeding at a density of 50,000 cells/cm^2 (n = 3/each time point/genotype). Cells were harvested for RNA extraction at days in the culture of 3, 9, and 16. On day 16, some plates were stained with Alizarin Red.

MC3T3-E1 subclone 14 osteoblast culture

MC3T3-E1 subclone 14 (M14) osteoblastic cells (Cell Culture Facility at UCSF) were seeded at an initial density of 50,000 cells/cm^2 and cultured with αMEM supplemented with 10% FBS, 1% P/S, 50 μg/μl AA, and 10 mM βGP in the humified CO_2 incubator at 37 °C. Cells were harvested for total RNA extraction at the days in the culture of 3, 9, 15, and 21.

Nfia *silencing*

MC3T3-E1 M14 osteoblastic cells were seeded at an initial density of 10,520 cells/cm^2 and cultured with αMEM supplemented with 10% FBS and 1% P/S. After 24 h of seeding, the medium was changed to αMEM supplemented with 10% FBS, 1% P/S, 50 μg/μl AA, and 10 mM βGP, and the cells were transfected with FlexiTube siRNA Premix for mouse *Nfia* (n = 4) (Qiagen) or AllStars negative control (n = 4) (Qiagen) according to manufacturer's instruction. The nontransduction group (n = 4) was used as a control. After additional 24 h of incubation, cells were harvested for the total RNA extraction.

Transducing lentivirus miR-exon4 inhibitor and establishing monoclonal subclones

MC3T3-E1M14 cells were plated (2.25×10^5 cells per 35 mm dish) and incubated with αMEM (without AA) supplemented with 10% FBS and 1% P/S. After 24 h, purified lentivirus particles of miR-exon4 inhibitor and negative control containing hygromycin selection marker (GeneCopoeia) were transduced to cells at a multiplicity of infection of 1:5 in the culture medium of αMEM supplemented with 10% FBS and 8 μg/ml polybrene (Santa Cruz Biotechnology). About 24 h later, the culture medium was changed to αMEM supplemented with 10% FBS and 1% P/S for another 24 h of incubation. Then, cells were incubated with αMEM with 10% FBS and 150 μl/ml hygromycin B for 9 days. On day 10 of selection culture, cells were trypsinized and replated to multiple dishes at two cells per well and incubated to develop monoclonal colonies with αMEM with 10% FBS and 200 μl/ml hygromycin B. Dishes with single colonies were maintained for colony expansion. Expanded monoclonal subclones (mi1-10 and negative control) were plated at a density of 50,000 cells/cm^2 and cultured with αMEM supplemented with 10% FBS, 1% P/S, 50 μg/μl AA, and 10 mM βGP. Cells were harvested for total RNA extraction at the days in the culture of 3, 9, 15, and 21 (n = 3/each time point/each subclone). At days in culture 2, 9, 16, and 23, cell proliferation and viability of each subclone were tested by 3-(4,5-dimethylthiazol-2-yl)-2,5-diphenyltetrazolium bromide (n = 3/each time point/each subclone) (Sigma–Aldrich) incorporation into viable cells using procedures recommended by the manufacturer. All incubations were done in the humidified 5% CO_2 incubator at 37 °C.

Extraction of RNA and miRNA and quantitative PCR analysis

Total RNA, including miRNA and mRNA, was using the Direct-zol RNA miniprep kit (Zymo Research). Selective reverse transcription of mature miRNA into complementary DNA was done using miScript II RT kit (Qiagen). Complementary DNA reverse transcribed from mRNA was obtained using Superscript IV First-Strand Synthesis Supermix for quantitative PCR (qPCR) (Thermo Fisher Scientific).

Expression of miRNA was characterized by qPCR with the miScript SYBR Green PCR Kit (Qiagen) and a custom-made primer for miR-exon4 (Qiagen), using the ABI 7500 system (Applied Biosystems). *Hs_RNU6-2* was used as a reference gene. Expression of mRNAs was examined by qPCR with TB Green Premix Ex Taq II (Takara Bio) using primer sets for *Runx2*, *Osx*, collagen type I alpha 1 chain, and *Nfia* (Elim Biopharmaceuticals). *Hmbs* (hydroxymethylbilane synthase) was used as a reference gene. Primer sequences are listed in Table S1. The relative expression levels of target genes were analyzed by the ΔΔCt method (51). The expression of each gene was calculated as a relative expression level (fold change) compared with nontransduced control and negative control (MC3T3-E1 subclones) or WT (primary osteoblasts). The significance of differences was determined by the two-tailed multiple *t* tests with Bonferroni correction following ANOVA (50). For the experiment with primary osteoblasts, the significance of differences was determined by independent Student's *t* test following *F* test. For both analyses, $p < 0.05$ was considered significantly different.

SDS-PAGE and Western blotting

Cultured MC3T3-E1 cell layers were harvested in radioimmunoprecipitation buffer on days of 3 or 9 of culture (n = 3/each time point/each subclone). Cells were homogenized by ultrasonication and centrifuged, and the supernatant was used for further analysis. Protein concentrations were determined using the bicinchoninic acid protein assay kit (Thermo Fisher Scientific). About 10 or 30 mg of protein per lane was separated on 4 to 15% gradient acrylamide gels under reducing conditions and transferred onto polyvinylidene difluoride membranes. Membranes were blocked with Odyssey blocking buffer (LI-COR Biosciences) for 1 h at room temperature followed by overnight incubation with rabbit anti-NFI/A antibody (Thermo Fisher Scientific; catalog no.: PA5-35936), rabbit anti-human mTOR antibody (Cell Signaling Technology; catalog no.: 2983), rabbit antihuman phosphorylated (Ser2448)-mTOR antibody (Cell Signaling Technology; catalog no.: 5536), and mouse antimouse GAPDH antibody (Proteintech Group; catalog no.: 60004-1-Ig) at 4 °C. Some membranes were stained with Revert 700 total protein stain kit (LI-COR Biosciences) prior to the blocking.

IRDye 680- or 800-conjugated Donkey anti-rabbit antibody and IRDye 800-conjugated donkey antimouse antibody (LI-COR Biosciences) were used as the secondary antibodies for an incubation of 1 h at room temperature. Bands were visualized by Odyssey CLx (LI-COR Biosciences) scanner, and band signal was analyzed using Image Studio software (LI-COR Biosciences). Signals of the bands were normalized by either total protein or GAPDH signals. Normalized band signals were statistically analyzed by independent Student's *t* test following *F* test. $p < 0.05$ was considered significantly different.

Quantitative proteomics

On day 3 of culture, nontransduced control (n = 3) and subclone mi2 (n = 3) of MC3T3-E1 M14 osteoblasts were harvested, and protein was extracted by homogenizing the cells in the radioimmunoprecipitation buffer. Protein concentrations were determined using the bicinchoninic acid protein assay kit (Thermo Fisher Scientific). Proteins were reduced by 10 mM Tris(2-carboxyethyl)phosphine (pH 7.0) at 56 °C for 1 h, followed by an alkylation treatment by 20 mM iodoacetamide at room temperature in the dark for 1 h. The treated proteins were precipitated in acetone overnight at −20 °C and reconstituted in 50 mM triethylamine bicarbonate buffer (pH 8.5) for trypsin digestion overnight at 37 °C. The digested peptides were labeled with tandem mass tag using TMT10plex Isobaric Label Reagent Set (Thermo Fisher Scientific) according to the manufacturer's instruction. The labeled peptides were dissolved in 0.1% TFA solution and fractionated using Pierce High pH Reversed-Phase Peptide Fractionation Kit (Thermo Fisher Scientific). Liquid contents

of each collected fraction were evaporated using vacuum centrifugation. The labeled peptides were analyzed by nano LC–MS/MS using an Orbitrap Fusion Lumos Tribrid Mass Spectrometer coupled with the EASY-nLC 1000 nanoflow Ultra Performance Liquid Chromatography system (Thermo Fisher Scientific). The peptides from each fraction were reconstituted in 0.1% formic acid (totaling 5 μl) and loaded on a 100 μm × 10 cm in-house made column packed with a reversed-phase ReproSil-Pur C18-AQ resin (3 μm, 120 Å, Dr Maisch GmbH) with the mobile phase as solvent A as 0.1% formic acid in water and solvent B as 0.1% formic acid in 100% acetonitrile. Peptides were resolved at 600 nl/min flow rate using a linear gradient from 4% to 10% solvent B for 10 min, from 10% to 22% for 95 min, from 22% to 40% for 35 min, from 40% to 95% for 5 min, and from 95% to 95% for 5 min. The mass spectrometry (MS) was done with the setting of the spray voltage 2.2 kV and temperature of the heated transfer capillary 270 °C. An MS survey scan was obtained for the *m/z* range 300 to 1650 and acquired with an orbitrap resolution of 60,000 with a total of 3 s per cycle at top speed mode. The top 16 most intense signals in the MS spectra were selected for further MS–MS analysis. MS–MS spectra were acquired in the linear ion trap using collision-induced dissociation for fragmentation at 40% energy with an activation Q of 0.25 with an activation time of 10 ms. The automatic gain control target values for full-scan modes were set to 1×10^4 ions or a maximum injection time of 30 ms. An isolation mass window of 3.0 *m/z* was used for precursor ion selection, charge states 2 to 6 were accepted, and a 30 s duration was used for dynamic exclusion.

The MS files were analyzed and searched against the mouse UniProt/Swiss-Prot protein database (release 2018_10; 17000 entries) using Proteome Discover, version 2.1 (Thermo Fisher Scientific). The parameters were set as follows: the protein modifications were carbamidomethylation (C) (fixed), oxidation (M) (variable); the enzyme specificity was set to trypsin; the maximum missed cleavages were set to two; the precursor ion mass tolerance was set to 10 ppm, and MS–MS tolerance was 20 ppm. A false discovery rate of ≤0.01 was applied to the MS results for following protein identification analysis. Differential protein abundance between nontransduced samples (biological replicate, n = 3) and mi2 (biological replicate, n = 3) was analyzed by independent Student's *t* test. A quantitative ratio over 1.5 ($p < 0.05$) was considered significant upregulation.

Data availability

All data generated or analyzed during this study are included in this article and its supporting information files.

Supporting information—This article contains supporting information.

Author contributions—Y. N. conceptualization; R. Z., G. L., D. A. U., M. L., and Y. N. methodology; Y. N. validation; R. Z., G. L., D. A. U., and M. L. formal analysis; R. Z., G. L., D. A. U., and M. L. investigation; Y. N. writing–original draft; R. Z., G. L., D. A. U., and M. L. writing–review & editing; Y. N. project administration; Y. N. funding acquisition.

Funding and additional information—This study was supported by funding from the School of Dentistry (to Y. N.), the Department of Orofacial Sciences (to Y. N.), the UCSF Center for Children's Oral Health Research (to Y. N.), and the National Institute of Dental and Craniofacial Research; grant no.: 5R01DE027366; to Y. N. The content is solely the responsibility of the authors and does not necessarily represent the official views of the National Institutes of Health.

Conflict of interest—The authors declare that they have no conflicts of interest with the contents of this article.

Abbreviations—The abbreviations used are: AA, ascorbic acid; ALPase, alkaline phosphatase; *Amel*, amelogenin; EGFP, enhanced GFP; FBS, fetal bovine serum; βGP, beta-glycerophosphate; IPA, Ingenuity pathway analysis; αMEM, alpha minimum essential medium; MS, mass spectrometry; mTOR, mechanistic target of rapamycin kinase; NFI/A, nuclear factor I/A; *Osx*, osterix; P5, postnatal 5; PKCη, protein kinase C-eta; P/S, penicillin/streptomycin; *Prkch*, PKCη gene; qPCR, quantitative PCR; *Runx2*, Runt-related transcription factor 2; SEAP, secreted alkaline phosphatase; UCSF, University of California, San Francisco.

References

1. Atsawasuwan, P., Lu, X., Ito, Y., Chen, Y., Gopinathan, G., Evans, C. A., Kulkarni, A. B., Gibson, C. W., Luan, X., and Diekwisch, T. G. H. (2013) Expression and function of enamel-related gene products in calvarial development. *J. Dent. Res.* **92**, 622–628
2. Jacques, J., Hotton, D., De la Dure-Molla, M., Petit, S., Asselin, A., Kulkarni, A. B., Gibson, C. W., Brookes, S. J., Berdal, A., and Isaac, J. (2014) Tracking endogenous amelogenin and ameloblastin *in vivo*. *PLoS One* **9**, e99626
3. Deutsch, D., Haze-Filderman, A., Blumenfeld, A., Dafni, L., Leiser, Y., Shay, B., Gruenbaum-Cohen, Y., Rosenfeld, E., Fermon, E., Zimmermann, B., Haegewald, S., Bernimoulin, J.-P., and Taylor, A. L. (2006) Amelogenin, a major structural protein in mineralizing enamel, is also expressed in soft tissues: Brain and cells of the hematopoietic system. *Eur. J. Oral Sci.* **114**, 183–189
4. Warotayanont, R., Frenkel, B., Snead, M. L., and Zhou, Y. (2009) Leucine-rich amelogenin peptide induces osteogenesis by activation of the Wnt pathway. *Biochem. Biophys. Res. Commun.* **387**, 558–563
5. Wen, X., Cawthorn, W. P., MacDougald, O. A., Stupp, S. I., Snead, M. L., and Zhou, Y. (2011) The influence of Leucine-rich amelogenin peptide on MSC fate by inducing Wnt10b expression. *Biomaterials* **32**, 6478–6486
6. Le, T. Q., Zhang, Y., Li, W., and Denbesten, P. K. (2007) The effect of LRAP on enamel organ epithelial cell differentiation. *J. Dent. Res.* **86**, 1095–1099
7. Jegat, N., Septier, D., Veis, A., Poliard, A., and Goldberg, M. (2007) Short-term effects of amelogenin gene splice products A+4 and A-4 implanted in the exposed rat molar pulp. *Head Face Med.* **3**, 40
8. Simmer, J. P., Hu, C. C., Lau, E. C., Sarte, P., Slavkin, H. C., and Fincham, A. G. (1994) Alternative splicing of the mouse amelogenin primary RNA transcript. *Calcif. Tissue Int.* **55**, 302–310
9. Ye, L., Le, T. Q., Zhu, L., Butcher, K., Schneider, R. A., Li, W., and Besten, P. K. D. (2006) Amelogenins in human developing and mature dental pulp. *J. Dent. Res.* **85**, 814–818
10. Sire, J. Y., Huang, Y., Li, W., Delgado, S., Goldberg, M., and Denbesten, P. K. (2012) Evolutionary story of mammalian-specific amelogenin exons 4, "4b", 8, and 9. *J. Dent. Res.* **91**, 84–89

11. Le, M. H., Warotayanont, R., Stahl, J., Den Besten, P. K., and Nakano, Y. (2016) Amelogenin Exon4 forms a novel miRNA that directs ameloblast and osteoblast differentiation. *J. Dent. Res.* **95**, 423–429
12. Michon, F., Tummers, M., Kyyronen, M., Frilander, M. J., and Thesleff, I. (2010) Tooth morphogenesis and ameloblast differentiation are regulated by micro-RNAs. *Dev. Biol.* **340**, 355–368
13. Bartel, D. P. (2004) MicroRNAs: Genomics, biogenesis, mechanism, and function. *Cell* **116**, 281–297
14. Kim, V. N., Han, J., and Siomi, M. C. (2009) Biogenesis of small RNAs in animals. *Nat. Rev. Mol. Cell Biol.* **10**, 126–139
15. Marsico, A., Huska, M. R., Lasserre, J., Hu, H., Vucicevic, D., Musahl, A., Orom, U., and Vingron, M. (2013) PROmiRNA: A new miRNA promoter recognition method uncovers the complex regulation of intronic miRNAs. *Genome Biol.* **14**, R84
16. Shapiro, J. L., Wang, H., Wen, X., Tannukit, S., and Paine, M. L. (2006) An amelogenin minigene to study alternative splicing. *DNA Cell Biol.* **25**, 1–5
17. Urbich, C., Kuehbacher, A., and Dimmeler, S. (2008) Role of microRNAs in vascular diseases, inflammation, and angiogenesis. *Cardiovasc. Res.* **79**, 581–588
18. Komori, T., Yagi, H., Nomura, S., Yamaguchi, A., Sasaki, K., Deguchi, K., Shimizu, Y., Bronson, R. T., Gao, Y. H., Inada, M., Sato, M., Okamoto, R., Kitamura, Y., Yoshiki, S., and Kishimoto, T. (1997) Targeted disruption of Cbfa1 results in a complete lack of bone formation owing to maturational arrest of osteoblasts. *Cell* **89**, 755–764
19. Yamamoto, H., Sakae, T., and Davies, J. E. (1989) Cleidocranial dysplasia: A light microscope, electron microscope, and crystallographic study. *Oral Surg. Oral Med. Oral Pathol.* **68**, 195–200
20. Fukuta, Y., Totsuka, M., Fukuta, Y., Takeda, Y., Yoshida, Y., Niitsu, J., and Yamamoto, H. (2001) Histological and analytical studies of a tooth in a patient with cleidocranial dysostosis. *J. Oral Sci.* **43**, 85–89
21. da Cunha, L. F., Caetano, I. M., Dalitz, F., Gonzaga, C. C., and Mondelli, J. (2014) Cleidocranial dysplasia case report: Remodeling of teeth as aesthetic restorative treatment. *Case Rep. Dent.* **2014**, 901071
22. Chu, Q., Gao, Y., Gao, X., Dong, Z., Song, W., Xu, Z., Xiang, L., Wang, Y., Zhang, L., Li, M., and Gao, Y. (2018) Ablation of Runx2 in ameloblasts suppresses enamel maturation in tooth development. *Sci. Rep.* **8**, 9594
23. Selbach, M., Schwanhausser, B., Thierfelder, N., Fang, Z., Khanin, R., and Rajewsky, N. (2008) Widespread changes in protein synthesis induced by microRNAs. *Nature* **455**, 58–63
24. Zambotti, A., Makhluf, H., Shen, J., and Ducy, P. (2002) Characterization of an osteoblast-specific enhancer element in the CBFA1 gene. *J. Biol. Chem.* **277**, 41497–41506
25. Wang, D., Christensen, K., Chawla, K., Xiao, G., Krebsbach, P. H., and Franceschi, R. T. (1999) Isolation and characterization of MC3T3-E1 preosteoblast subclones with distinct *in vitro* and *in vivo* differentiation/mineralization potential. *J. Bone Miner. Res.* **14**, 893–903
26. Arvey, A., Larsson, E., Sander, C., Leslie, C. S., and Marks, D. S. (2010) Target mRNA abundance dilutes microRNA and siRNA activity. *Mol. Syst. Biol.* **6**, 363
27. Hausser, J., and Zavolan, M. (2014) Identification and consequences of miRNA-target interactions–beyond repression of gene expression. *Nat. Rev. Genet.* **15**, 599–612
28. Linsley, P. S., Schelter, J., Burchard, J., Kibukawa, M., Martin, M. M., Bartz, S. R., Johnson, J. M., Cummins, J. M., Raymond, C. K., Dai, H., Chau, N., Cleary, M., Jackson, A. L., Carleton, M., and Lim, L. (2007) Transcripts targeted by the microRNA-16 family cooperatively regulate cell cycle progression. *Mol. Cell Biol.* **27**, 2240–2252
29. Llave, C., Xie, Z., Kasschau, K. D., and Carrington, J. C. (2002) Cleavage of Scarecrow-like mRNA targets directed by a class of Arabidopsis miRNA. *Science* **297**, 2053–2056
30. Yin, K., Hacia, J. G., Zhong, Z., and Paine, M. L. (2014) Genome-wide analysis of miRNA and mRNA transcriptomes during amelogenesis. *BMC Genomics* **15**, 998
31. Zhang, Y., Kim, J. Y., Horst, O., Nakano, Y., Zhu, L., Radlanski, R. J., Ho, S., and Den Besten, P. K. (2014) Fluorosed mouse ameloblasts have increased SATB1 retention and Gαq activity. *PLoS One* **9**, e103994
32. Lee, D. S., Roh, S. Y., and Park, J.-C. (2018) The Nfic-osterix pathway regulates ameloblast differentiation and enamel formation. *Cell Tissue Res.* **374**, 531–540
33. Lee, D. S., Choung, H. W., Kim, H. J., Gronostajski, R. M., Yang, Y. I., Ryoo, H. M., Lee, Z. H., Kim, H. H., Cho, E. S., and Park, J. C. (2014) NFI-C regulates osteoblast differentiation *via* control of osterix expression. *Stem Cells* **32**, 2467–2479
34. Oh, H. J., Lee, H. K., Park, S. J., Cho, Y. S., Bae, H. S., Cho, M. I., and Park, J. C. (2012) Zinc balance is critical for NFI-C mediated regulation of odontoblast differentiation. *J. Cell Biochem.* **113**, 877–887
35. Shalgi, R., Lieber, D., Oren, M., and Pilpel, Y. (2007) Global and local architecture of the mammalian microRNA–transcription factor regulatory network. *PLoS Comput. Biol.* **3**, e131
36. Tsang, J., Zhu, J., and van Oudenaarden, A. (2007) MicroRNA-mediated feedback and feedforward loops are recurrent network motifs in mammals. *Mol. Cell* **26**, 753–767
37. Yan, F., Jia, P., Yoshioka, H., Suzuki, A., Iwata, J., and Zhao, Z. (2020) A developmental stage-specific network approach for studying dynamic co-regulation of transcription factors and microRNAs during craniofacial development. *Development* **147**, dev192948
38. Shamimuzzaman, M., and Vodkin, L. (2012) Identification of soybean seed developmental stage-specific and tissue-specific miRNA targets by degradome sequencing. *BMC Genomics* **13**, 310
39. Chen, J., and Long, F. (2018) mTOR signaling in skeletal development and disease. *Bone Res.* **6**, 1
40. Singha, U. K., Jiang, Y., Yu, S., Luo, M., Lu, Y., Zhang, J., and Xiao, G. (2008) Rapamycin inhibits osteoblast proliferation and differentiation in MC3T3-E1 cells and primary mouse bone marrow stromal cells. *J. Cell Biochem.* **103**, 434–446
41. Djuranovic, S., Nahvi, A., and Green, R. (2012) miRNA-mediated gene silencing by translational repression followed by mRNA deadenylation and decay. *Science* **336**, 237–240
42. Bazzini, A. A., Lee, M. T., and Giraldez, A. J. (2012) Ribosome profiling shows that miR-430 reduces translation before causing mRNA decay in Zebrafish. *Science* **336**, 233–237
43. Béthune, J., Artus-Revel, C. G., and Filipowicz, W. (2012) Kinetic analysis reveals successive steps leading to miRNA-mediated silencing in mammalian cells. *EMBO Rep.* **13**, 716–723
44. Wang, X.-P., Åberg, T., James, M. J., Levanon, D., Groner, Y., and Thesleff, I. (2005) Runx2 (Cbfa1) inhibits Shh signaling in the lower but not upper molars of mouse embryos and prevents the budding of putative successional teeth. *J. Dent. Res.* **84**, 138–143
45. Takahashi, S., Kawashima, N., Sakamoto, K., Nakata, A., Kameda, T., Sugiyama, T., Katsube, K.-i., and Suda, H. (2007) Differentiation of an ameloblast-lineage cell line (ALC) is induced by Sonic hedgehog signaling. *Biochem. Biophys. Res. Commun.* **353**, 405–411
46. Seidel, K., Ahn, C. P., Lyons, D., Nee, A., Ting, K., Brownell, I., Cao, T., Carano, R. A., Curran, T., Schober, M., Fuchs, E., Joyner, A., Martin, G. R., de Sauvage, F. J., and Klein, O. D. (2010) Hedgehog signaling regulates the generation of ameloblast progenitors in the continuously growing mouse incisor. *Development* **137**, 3753–3761
47. Liu, X., and Gao, Y. (2013) Runx2 is involved in regulating amelotin promoter activity and gene expression in ameloblasts. In *2013 ICME International Conference on Complex Medical Engineering*
48. Lee, H. K., Lee, D. S., Ryoo, H. M., Park, J. T., Park, S. J., Bae, H. S., Cho, M. I., and Park, J. C. (2010) The odontogenic ameloblast-associated protein (ODAM) cooperates with RUNX2 and modulates enamel mineralization via regulation of MMP-20. *J. Cell Biochem.* **111**, 755–767
49. Gibson, C. W., Yuan, Z. A., Hall, B., Longenecker, G., Chen, E., Thyagarajan, T., Sreenath, T., Wright, J. T., Decker, S., Piddington, R., Harrison, G., and Kulkarni, A. B. (2001) Amelogenin-deficient mice display an amelogenesis imperfecta phenotype. *J. Biol. Chem.* **276**, 31871–31875
50. Yuan, J., Reed, A., Chen, F., and Stewart, C. N. (2006) Statistical analysis of real-time PCR data. *BMC Bioinformatics* **7**, 85
51. Livak, K. J., and Schmittgen, T. D. (2001) Analysis of relative gene expression data using real-time quantitative PCR and the 2−ΔΔCT method. *Methods* **25**, 402–408